This is a repository copy of *Understanding the eastward shift and intensification of the ENSO teleconnection over South Pacific and Antarctica under greenhouse warming*.

White Rose Research Online URL for this paper:
https://eprints.whiterose.ac.uk/224743/

Version: Published Version

Article:

Check for updates

Understanding the Eastward Shift and Intensification of the ENSO Teleconnection Over South Pacific and Antarctica Under Greenhouse Warming

Ya Wang [1,2,3], Gang Huang [1,2,3]*, Kaiming Hu [1,4]*, Weichen Tao [1], Hainan Gong [4], Kai Yang [1] and Haosu Tang [1]

[1]State Key Laboratory of Numerical Modeling for Atmospheric Sciences and Geophysical Fluid Dynamics, Institute of Atmospheric Physics, Chinese Academy of Sciences, Beijing, China, [2]Laboratory for Regional Oceanography and Numerical Modeling, Qingdao National Laboratory for Marine Science and Technology, Qingdao, China, [3]University of Chinese Academy of Sciences, Beijing, China, [4]Center for Monsoon System Research, Institute of Atmospheric Physics, Chinese Academy of Sciences, Beijing, China

The Pacific–South America (PSA) teleconnection pattern triggered by the El Niño/Southern Oscillation (ENSO) is suggested to be moving eastward and intensifying under global warming. However, the underlying mechanism is not completely understood. Previous studies have proposed that the movement of the PSA teleconnection pattern is attributable to the eastward shift of the tropical Pacific ENSO-driven rainfall anomalies in response to the projected El Niño-like sea surface temperature (SST) warming pattern. In this study, we found that with uniform warming, models will also simulate an eastward movement of the PSA teleconnection pattern, without the impact of the uneven SST warming pattern. Further investigation reveals that future changes in the climatology of the atmospheric circulation, particularly the movement of the exit region of the subtropical jet stream, can also contribute to the eastward shift of the PSA teleconnection pattern by modifying the conversion of mean kinetic energy to eddy kinetic energy.

Keywords: El Niño/Southern oscillation, Global Warming, Subtropical Jet Stream, Pacific–South American teleconnection pattern, ENSO teleconnection

INTRODUCTION

The El Niño/Southern Oscillation (ENSO), as the primary interannual air-sea coupled mode in the tropical Pacific, has significant effects on the global climate variability (Hoerling et al., 1997; Horel and Wallace 1981; Hu et al., 2021; Liu and Alexander 2007; Trenberth et al., 1998; Xie et al., 2016; Straus and Shukla 2002; Yang et al., 2018; Sun et al., 2019; Sun et al., 2022). The ENSO has a three-pronged effect on the climate variability in the extratropics of the Southern Hemisphere. To begin, El Niño events warm the tropical atmosphere at all longitudes, resulting in the strengthening and equatorward movement of the subtropical jet stream (STJ) and descending branches of the Hadley circulation (Rind et al., 2001; Seager et al., 2003; Lu et al., 2008). Second, ENSO can affect the Southern Hemisphere Annular Mode by influencing the propagation and intensity of transient eddies (Fogt et al., 2011; L'Heureux and Thompson 2006; Lau and Lau 1992; Lau et al., 2005; Seager et al., 2003). Third, the ENSO signal is capable of propagating to mid- and high-latitudes, as well as to
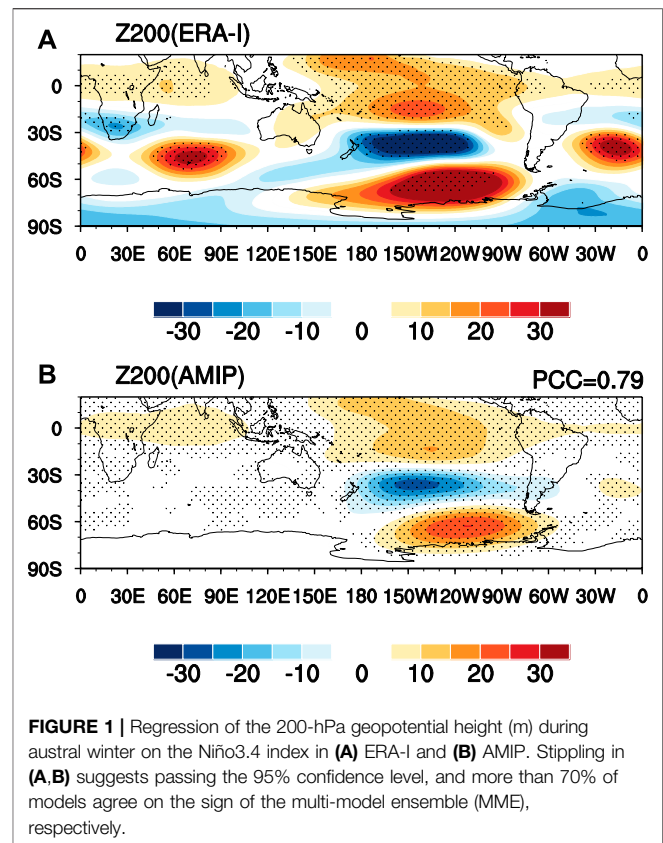
TABLE 1 | AMIP models from CMIP6 used in this study.

Model	Institute
BCC-CSM2-MR	Beijing Climate Center, China
CanESM5	Canadian Centre for Climate Modelling and Analysis, Canada
CESM2	National Center for Atmospheric Research, USA
CNRM-CM6-1	Centre National de Recherches Meteorologiques, France
GFDL-CM4	National Oceanic and Atmospheric Administration, Geophysical Fluid Dynamics Laboratory, USA
IPSL-CM6A-LR	L'Institut Pierre-Simon Laplace, France
MRI-ESM2-0	Meteorological Research Institute, Japan
MIROC6	The University of Tokyo, National Institute for Environment Studies, and Japan Agency for Marine-Earth Science and Technology, Japan

Antarctica, *via* stationary waves generated by the anomalous tropical convection in the tropical Pacific (Held et al., 2002; Schneider et al., 2012). In the Southern Hemisphere, the ENSO teleconnection resembles the Pacific–South American (PSA) wave train characterized by alternating pressure centers east of New Zealand, near the Amundsen Sea and South America, curving poleward and eastward toward Antarctica, highly impacting the depth of the Amundsen Sea Low (Karoly 1989; Mo and Higgins 1998; Mo and Paegle 2001; Schneider et al., 2012). The variability of the Amundsen Sea Low could further modulate the temperature and sea ice anomalies over Antarctica (Yuan and Martinson 2000; Yuan 2004; Li et al., 2015; Wang et al., 2020; Wang et al., 2022).

The PSA teleconnection pattern triggered by ENSO events is strongly seasonally dependent and is zonally asymmetric during El Niño and La Niña years (Jin and Kirtman 2009; Hitchman and Rogal 2010; Ding et al., 2012; Schneider et al., 2012; Li et al., 2021). The seasonality of the PSA being more pronounced in austral winter and spring is primarily attributable to the seasonal variation in the STJ. A stronger and more equatorward STJ in austral winter and spring favors the formation of the Rossby wave source (Sardeshmukh and Hoskins 1988) in the subtropical Pacific, resulting in a more pronounced PSA teleconnection pattern (Jin and Kirtman 2009; Scott Yiu and Maycock, 2019). The asymmetric impacts between the warm and cold phase of ENSO, which exhibit a more eastward PSA wave train during El Niño than La Niña, can be attributable to the shift of the anomalous tropical convection and the discrepancy of the STJ (Hoerling et al., 1997; Wang et al., 2021; Wang et al., 2022).

Under global warming, Pacific–North American (PNA) and the PSA teleconnection pattern triggered by ENSO events are both projected to move eastward and intensify (Zhou et al., 2014; Cai et al., 2021). Previous studies have proposed that the movement of the teleconnection pattern is attributable to the eastward shift of the ENSO-driven rainfall anomalies over the tropical Pacific in response to the projected El Niño-like warming pattern (Zhou et al., 2014; Cai et al., 2021; Hu et al., 2021). As a result of the overall reduction of the tropical circulations due to the increased

FIGURE 1 | Regression of the 200-hPa geopotential height (m) during austral winter on the Niño3.4 index in (A) ERA-I and (B) AMIP. Stippling in (A,B) suggests passing the 95% confidence level, and more than 70% of models agree on the sign of the multi-model ensemble (MME), respectively.

static stability in the tropics under greenhouse warming, the tropical Pacific sea surface temperature (SST) change features an El Niño-like warming pattern (Held and Soden 2006; Huang and Xie 2015; Yeh et al., 2018). The background warming pattern, in turn, results in the intensification and the eastward movement of the ENSO-driven rainfall anomalies in the tropical Pacific (Power et al., 2013; Huang and Xie 2015). In response to the changes in the ENSO-driven rainfall anomalies, the extratropical Rossby wave trains, as the PSA and PNA teleconnection pattern, are projected to shift eastward and strengthen in previous studies (Cai et al., 2021; Zhou et al., 2014; Yeh et al., 2018).

In addition to tropical heating anomalies, the PSA teleconnection pattern is modulated by the extratropical circulation (Meehl et al., 2007; Muller and Roeckner 2008). Several early (Simmons et al., 1983; Ting and Yu 1998) and recent studies (Wang et al., 2021; Wang et al., 2022) have suggested that the STJ is critical in determining the position of extratropical ENSO teleconnections. Here, we showed that the eastward shift of the PSA teleconnection pattern is presented even without the impact of the uneven SST warming pattern, in which the future change of climatological circulation plays an important role.

The remainder of this study is organized as follows: **Section 2** introduces data and methods. **Section 3** presents the results involving the changes in the teleconnection pattern and the underlying mechanisms. **Section 4** provides a summary.
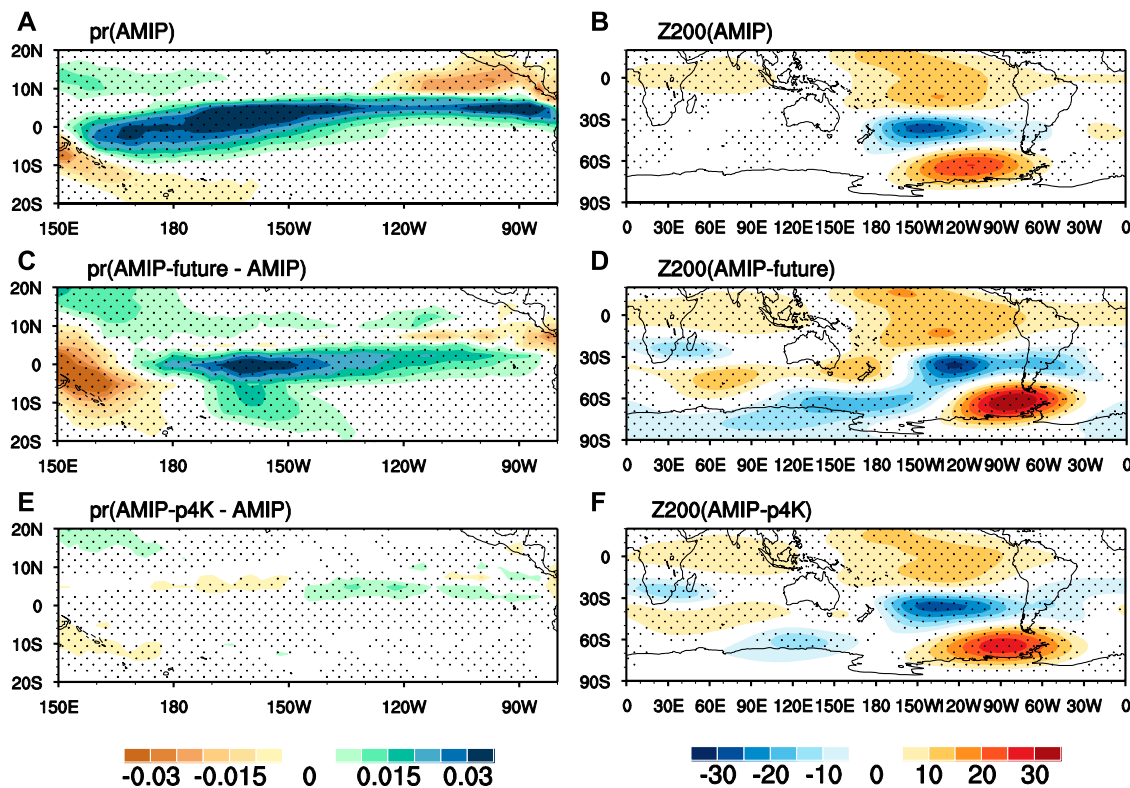
FIGURE 2 | Simulated ENSO-driven rainfall anomalies (mm/day, left column) and ENSO-driven geopotential height anomalies (m, right column) in **(A,B)** AMIP, **(C,D)** AMIP-future4K, and **(E,F)** AMIP-p4K MME. The precipitation anomalies in **(C,E)** denote the precipitation change compared to AMIP. Stippling denotes that more than 70% of models agree on the sign of the MME.

DATA AND METHODS

a. Reanalysis and model data

To investigate the future change of the ENSO-triggered PSA teleconnection pattern under global warming, a set of atmospheric-only experiments from the phase 6 of the Coupled Model Intercomparison Project (CMIP6) is utilized. The experiments, namely, AMIP, AMIP-p4K with uniform warming, and AMIP-future4K with patterned warming, are simulated by the atmospheric general circulation models. AMIP is forced by the observed monthly sea ice and SST; the latter two are forced by the observed SST anomalies and the uniform SST, and patterned climatological SST obtained from CMIP5 ensemble mean SST changes at $4 \times CO_2$, respectively. The details of the models are listed in **Table 1**.

In this study, the July–August (JJA) mean geopotential height is derived from the European Centre for Medium-Range Weather Forecasts Interim Reanalysis (ERAI; Berrisford et al., 2011) at a resolution of $2.5° \times 2.5°$ from 1979 to 2014. The Niño 3.4 index is from the climate prediction center of NOAA (https://www.cpc.ncep.noaa.gov/), and the principal component of the first empirical orthogonal functional mode of the SST over the

tropical Pacific (120°E–80°W, 15°S–15°N) is defined as the Niño index in the AMIP simulations. Regression analysis is used, and the statistical significance of this study is evaluated by the two-tailed Student's t-test.

b. Linearized Baroclinic Model (LBM)

The LBM used in this study is based upon the primitive equations linearized at a given state with a horizontal resolution of T42 and 20 sigma levels and schemes for horizontal and vertical diffusion, Rayleigh friction, and Newtonian damping. This model is widely used and has an irreplaceable role in the study of climate dynamics (Xie et al., 2009; Hu et al., 2019). More details of the model are presented in Watanabe and Kimoto (2000). To produce a stable atmospheric response to the heating forcing, the model is integrated for 50 days, and the average from the 20th to 50th day is used for analysis.

c. Kinetic energy conversion

As stated by Kosaka and Nakamura (2006), the barotropic growth of the local kinetic energy associated with perturbations from the basic state is given by
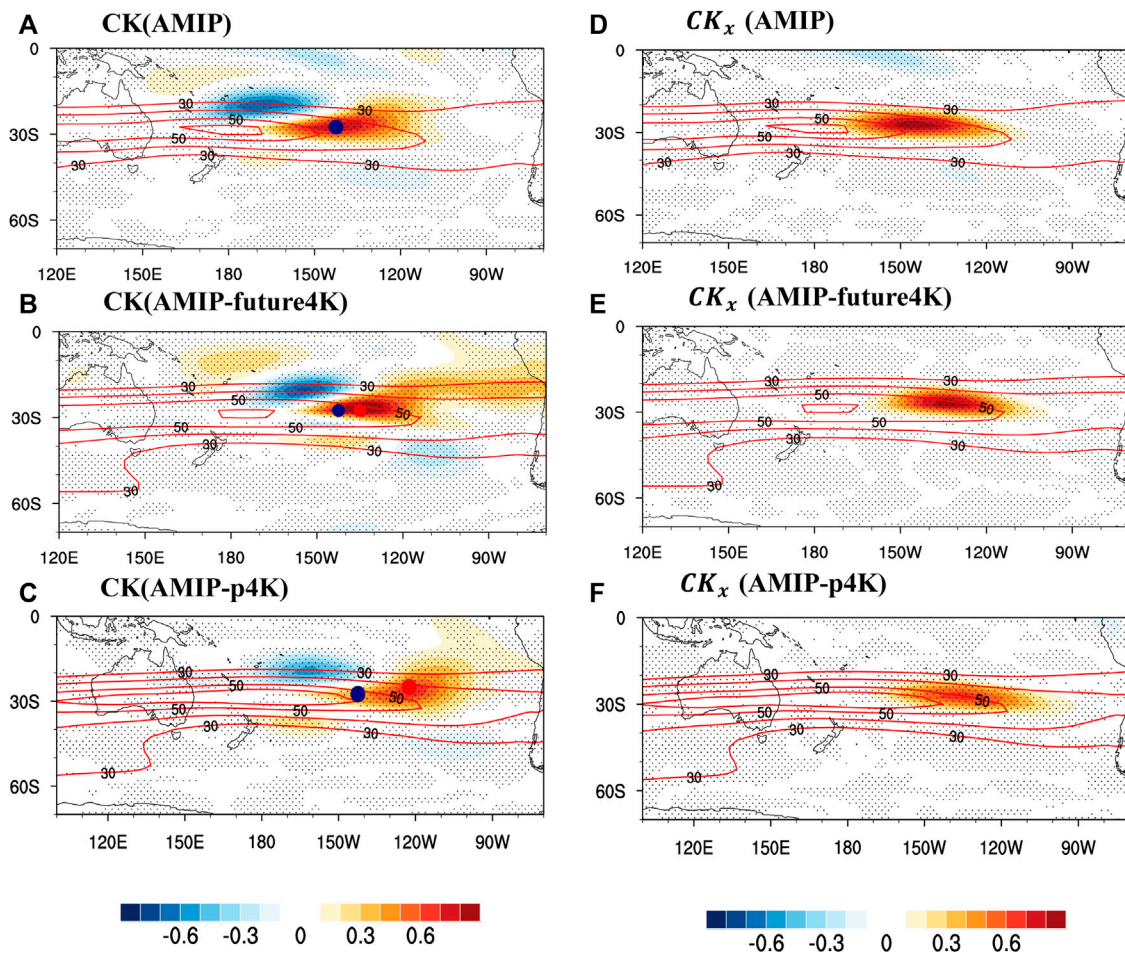
FIGURE 3 | MME of the JJA climatological zonal wind (contour lines; m/s) and CK (shading in a–c; m²/s³) and CKₓ (shading in d–f; m²/s³) in **(A,D)** AMIP, **(B,E)** AMIP-future4K, and **(C,F)** AMIP-p4K. The dots indicate that more than 70% of models agree on the sign of the MME. The navy dot denotes the central position of the CK in the mid-latitudes in AMIP, and the red dots in **(B,C)** denote the central position of the CK in the mid-latitudes in AMIP-future4K and AMIP-p4K, respectively. **(C)** Role of the STJ.

$$\frac{\partial KEH}{\partial t} \approx \underbrace{\frac{\left(v'^2 - u'^2\right)}{2}\left(\frac{\partial \bar{u}}{\partial x} - \frac{\partial \bar{v}}{\partial y}\right)}_{CK_x} - \underbrace{u'v'\left(\frac{\partial \bar{u}}{\partial y} + \frac{\partial \bar{v}}{\partial x}\right)}_{CK_y}. \quad (1)$$

Here, u' and v' are the anomalous zonal and meridional winds, respectively. $\bar{u}$ and $\bar{v}$ denote the zonal and meridional climatological winds, respectively. KEH is horizontal perturbed kinetic energy, and CK (the sum of CK_x and CK_y) is the conversion of local kinetic energy from the basic state to atmospheric anomalies.

RESULTS

a. Evaluation of the AMIP simulations of the ENSO-triggered PSA teleconnection pattern.

The atmospheric anomalies triggered by ENSO during austral winter are depicted in **Figure 1** in observations and AMIP. In the

tropical Pacific, the anomalous convective heating excites a Gill-like response (**Figure 1A**). The extratropical teleconnection pattern resembles the PSA wave train, characterized by an anomalous low-pressure center east of New Zealand, a high-pressure anomaly near the Amundsen Sea in the Pacific sector. The structure of the atmospheric responses to ENSO in the AMIP is comparable to that observed with a pattern correlation coefficient between atmospheric anomalies in ERAI and AMIP (0–90°S; 0–360°) of up to 0.79. The resemblance shows that the AMIP models are capable of simulating the ENSO teleconnection in the Southern Hemisphere. It should be noted that the intensity of the PSA teleconnection pattern in AMIP is weaker than observed, suggesting that there may be some common bias in AMIP models, but this inaccuracy does not affect our conclusions as we mainly made comparisons between different AMIP experiments. As a result, it is feasible to undertake subsequent investigations using these simulations.

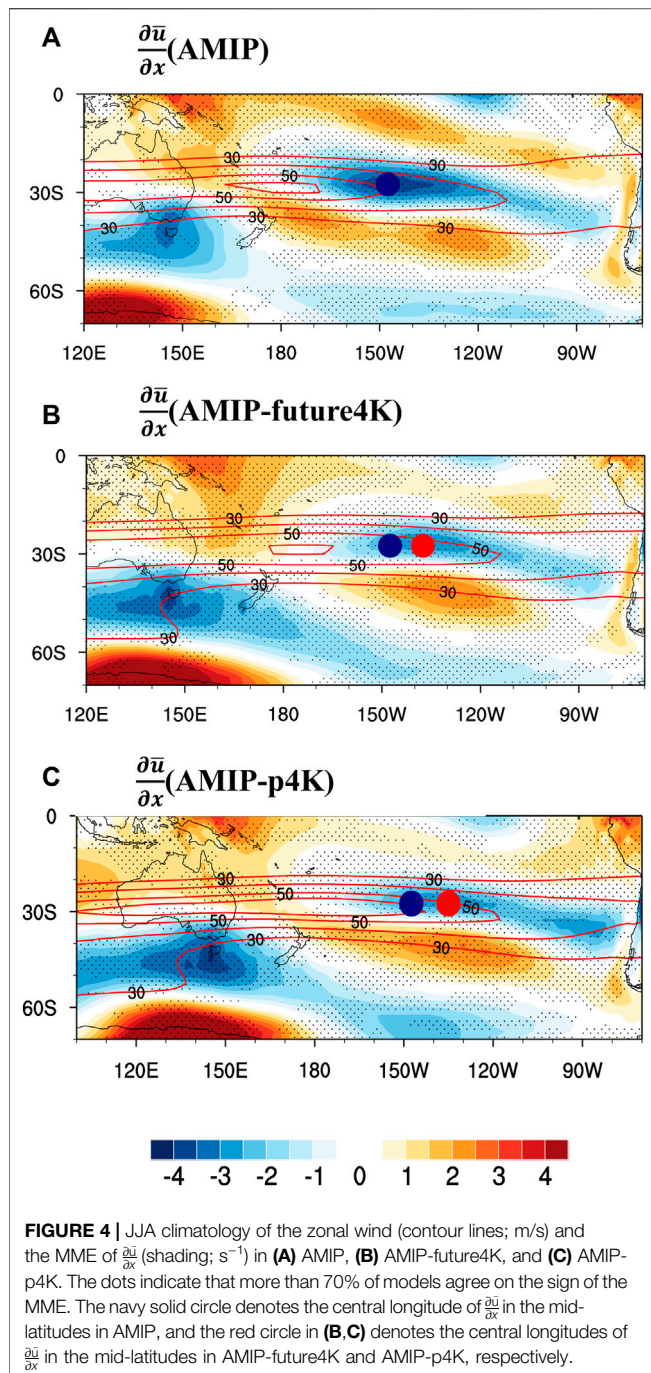b. Results in AMIP-p4K and AMIP-future4K

FIGURE 4 | JJA climatology of the zonal wind (contour lines; m/s) and the MME of $\frac{\partial \bar{u}}{\partial x}$ (shading; s^{-1}) in **(A)** AMIP, **(B)** AMIP-future4K, and **(C)** AMIP-p4K. The dots indicate that more than 70% of models agree on the sign of the MME. The navy solid circle denotes the central longitude of $\frac{\partial \bar{u}}{\partial x}$ in the mid-latitudes in AMIP, and the red circle in **(B,C)** denotes the central longitudes of $\frac{\partial \bar{u}}{\partial x}$ in the mid-latitudes in AMIP-future4K and AMIP-p4K, respectively.

Figure 2A presents the ENSO-driven rainfall anomalies in the tropical Pacific in AMIP. Positive responses are distributed in the eastern and central Pacific, whereas negative responses are found on the north flank of the equatorial eastern Pacific which is mainly contributed by the anomalous dry advection (Su and Neelin 2002). In comparison to AMIP, ENSO-driven precipitation anomalies increase in the central and eastern Pacific in the AMIP-future4K and decrease in the western tropical Pacific, resulting in an overall eastward shift and amplification of the precipitation anomalies in the tropical

Pacific (**Figure 2C**). The changes between AMIP-future4K and AMIP are consistent with prior results based on the future simulations in CMIP5/6, which suggest that the El Niño-like warming pattern leads to an eastward shift and intensification of ENSO convective anomalies in the tropical Pacific (Huang and Xie 2015).

Compared with the PSA teleconnection pattern in AMIP, the experimental result from AMIP-future4K displays a more eastward and more intense PSA teleconnection pattern (**Figures 2B,D**). The concurrent intensification and the eastward movement of the ENSO-driven rainfall anomalies in the tropical Pacific and the PSA teleconnection pattern in AMIP-future4K are consistent with earlier studies (Zhou et al., 2014; Cai et al., 2021). When only the climatological SST differs between AMIP and AMIP-future4K, this discrepancy brings several additional changes, including changes in the water vapor, the position of ENSO-driven precipitation anomalies, and the background atmospheric circulation. Previous studies have suggested that all these factors may have an effect on the ENSO teleconnection pattern (Held and Soden 2006; Huang and Xie 2015; Hu et al., 2021).

To disentangle the above factors and examine the causal relationship between each factor and the future changes in the PSA teleconnection pattern, the AMIP-p4K experiment is further introduced for comparison. AMIP-p4K results show a minor increase in ENSO-driven rainfall anomalies over the northeastern tropical Pacific and a decrease in the central and southwestern Pacific relative to that in the AMIP experiment (**Figure 2E**). The amplitude of ENSO-driven rainfall anomalies over the tropical Pacific in AMIP-p4K is significantly smaller than that in AMIP-future4K and is insufficient to cause the eastward shift and intensification of ENSO-driven precipitation anomalies relative to that in AMIP.

By further comparing the circulation changes in AMIP-p4K and AMIP-future4K, we found that the El Niño-like warming pattern significantly intensifies the PSA wave train (**Figures 2D,F**). Corresponding to more intense precipitation anomalies in AMIP-future4K with the El Niño-like warming pattern, the strength of the PSA teleconnection pattern is significantly stronger than that in AMIP, whereas the PSA teleconnection pattern in AMIP-p4K is comparable to that in AMIP. The result demonstrates that the future climatological warming pattern contributes to the intensification of the ENSO-triggered PSA teleconnection pattern.

In terms of the movement of the PSA teleconnection pattern, despite the substantial difference in the climatological SST between the two experiments, the PSA teleconnection pattern shifts a comparable distance. This finding suggests that the causal link between the movement of the ENSO-driven rainfall anomalies in the tropical Pacific and the shift of the PSA wave train may be insufficiently robust, and other causes may potentially contribute to the shift of the PSA teleconnection pattern.

The STJ is critical in the development of the subtropical disturbance *via* barotropic energy conversion (Simmons et al., 1983), acting as an anchor for the location of the ex-tropical wave train triggered by the tropical heating (Ting and Yu 1998). The variation of the STJ plays an important role in the asymmetric
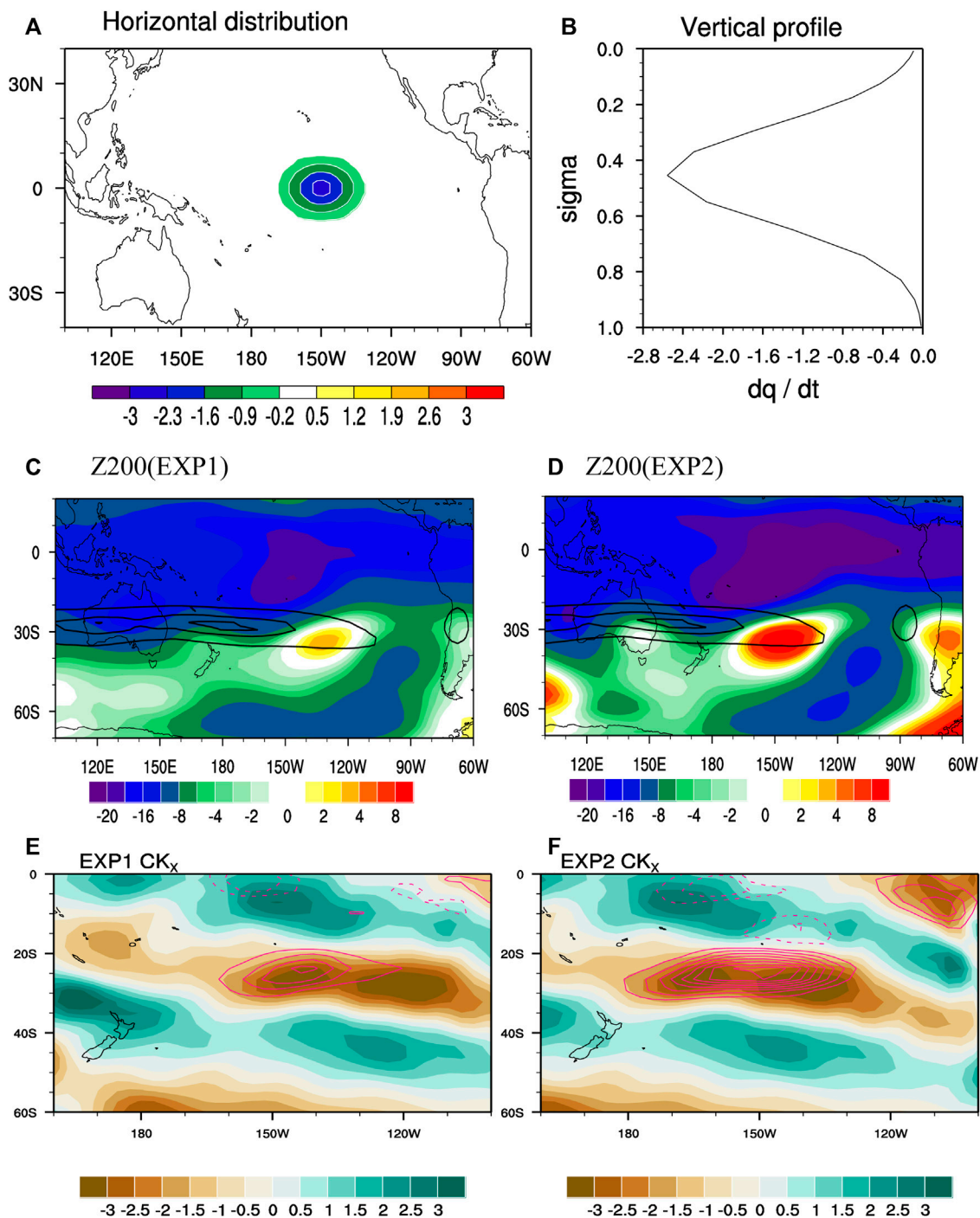
FIGURE 5 | (A) Horizontal distribution and **(B)** vertical profile of imposed atmospheric diabatic heating (K day^{-1}) in the central Pacific in the two LBM experiments. The climatological zonal wind (contour lines, m/s) and the 200-hPa geopotential height (shading, m) responded to the heating sources in **(C)** EXP1 and **(D)** EXP2. CK$_x$ (contour lines; m^2/s^3) and $\frac{\partial \bar{u}}{\partial x}$ (shading, s^{-1}) in **(E)** EXP1 and **(F)** EXP2. Adapted from Wang et al. (2022). © American Meteorological Society. Used with permission.

impacts of ENSO on the PSA teleconnection pattern by altering the barotropic energy conversion (Wang et al., 2021). In the following study, the movement of the PSA teleconnection pattern under global warming is investigated from the perspective of energy conversion.

Figure 3 presents the climatological zonal winds and the CK in three experiments. In AMIP, the positive CK at the exit of the STJ is consistent with the position of the atmospheric anomaly east of New Zealand (**Figures 2B, 3A**), indicating the importance of the CK in the development of the disturbance. The majority of the

positive CK at the exit of the STJ is contributed by CK_x (**Figures 3A,B**). According to **Eq. 1**, the zonally elongated ($u'>v'$) atmospheric anomaly east of New Zealand is eager to extract barotropic energy (CK_x) from the basic mean flow (**Figure 3A**) and develops at the exit region of the STJ where the mean zonal flow is confluent ($\frac{\partial \bar{u}}{\partial x} < 0$; **Figure 4A**).

In AMIP-future4K, the exit region of the STJ with substantial confluence shifts eastward at about 10° longitudes (**Figure 4B**). As the exit region of the STJ moves eastward (*see* the navy and red solid circles in **Figure 4B**), the strong positive CK favorable to the development of atmospheric anomalies move eastward in lockstep (*see* the navy and red solid circles in **Figure 3B**). Similar to AMIP-future4K, the eastward shift of the PSA teleconnection pattern in AMIP-p4K is accompanied by the movement of the STJ exit and the positive CK in the subtropical Pacific (**Figures 3C, 4C**).

The aforementioned result illustrates that the movement of the climatological STJ exit region contributes to the shift of the PSA teleconnection pattern. To further confirm the effect of STJ changes on the PSA teleconnection pattern, a set of LBM experiments are utilized for investigation, following Wang et al. (2022). The first LBM experiment (EXP1) is forced by the heating source centered at 150°W (**Figures 5A,B**) and the JJA climatological mean flow. The prescribed heating source has a cosine elliptical pattern, with a peak of $-3\,K\,day^{-1}$ at the 0.45 sigma level. The horizontal distribution and the vertical profile of the heating source are presented in **Figures 5A,B**, respectively. The second experiment (EXP2) utilizes the same heating source but shifts the mean flow 20° longitude westward, mimicking the movement of the STJ exit region. In EXP1, the atmospheric response to the tropical heating in the subtropical Pacific is centered at the exit of the STJ, where the climatological zonal flow is significantly confluent (**Figures 5C,D**). Similar to the experimental results in AMIP experiments, the strong positive CK which contributes to the development of the disturbance is detected at the exit of the STJ in EXP1. However, in EXP2, with the same tropical heating source, the strong positive CK in the mid-latitudes moves westward, paralleling the change of the exit of the climatological STJ (**Figure 5D**). The consistent movement of the positive CK and disturbance in the subtropical Pacific (**Figures 5E,F**) demonstrate that the movement of the STJ exit region causes a shift in the position of the PSA teleconnection pattern by modifying the conversion of mean kinetic energy to eddy kinetic energy.

CONCLUSION AND DISCUSSION

In this study, the underlying mechanisms of the eastward shift and intensification of the ENSO-triggered PSA teleconnection pattern under global warming are investigated based on a set of AMIP experiments from CMIP6.

By comparing the AMIP-p4K and AMIP-future4K, it is found that the El Niño-like warming significantly intensifies the PSA wave train. Corresponding to more intense precipitation anomalies over tropical Pacific in AMIP-future4K with patterned warming, the strength of the PSA teleconnection

pattern is significantly stronger than that in AMIP, whereas the PSA teleconnection pattern in AMIP-p4K with uniform warming is comparable to that in AMIP.

We found that the PSA teleconnection pattern triggered by ENSO will still shift eastward under global warming with the absence of El Niño-like SST warming. Despite the significant difference in the climatological SST between AMIP-p4K and AMIP-future4K, the PSA teleconnection pattern shifts a comparable distance in the two experiments relative to that in AMIP. Further investigation reveals that changes in the climatological STJ, particularly the movement of the exit region of the STJ, can significantly affect the position of the PSA teleconnection pattern by influencing the conversion of mean kinetic energy to eddy kinetic energy. The eastward shift of the exit region of the Pacific STJ in both experiments causes the position where the disturbance is most likely to develop to move eastward, which in turn leads to the eastward shift of the PSA teleconnection pattern. Our results, therefore, emphasize the importance of the climatological circulation change on the projected eastward shift of the PSA teleconnection pattern.

The mechanism proposed in this study complements the previous mechanism (Cai et al., 2021; Kug et al., 2010; Meehl et al., 2007; Muller and Roeckner, 2008; Zhou et al., 2014), and taken together, they may collectively contribute to the eastward shift of the PSA teleconnection pattern. This study is based on AMIP experiments which do not incorporate air–sea coupling processes; further research using the coupled model should be conducted in the future to better understand the issue and quantify the contributions of the STJ, SST warming pattern, and the CO_2 direct radiation to the eastward movement and the intensification of the ENSO-triggered PSA teleconnection pattern.

DATA AVAILABILITY STATEMENT

The data that supports the finding of this study is openly available at https://www.ecmwf.int/en/forecasts/datasets/reanalysis-datasets (ERAI; Berrisford et al., 2011), and https://esgf-node.llnl.gov/search/cmip6/ (CMIP6).

AUTHOR CONTRIBUTIONS

YW, GH, and KH conceived the study, performed the analyses, built the mechanism, and wrote the manuscript. WT, HG, KY, and HT contributed to improving the manuscript and assisted in the interpretation of the results.

FUNDING

REFERENCES

Berrisford, P., Dee, D. P., Poli, P., Brugge, R., Fielding, M., Fuentes, M., et al. (2011). *The ERA-Interim Archive, Version 2.0*.

Cai, W., Santoso, A., Collins, M., Dewitte, B., Karamperidou, C., Kug, J.-S., et al. (2021). Changing El Niño-Southern Oscillation in a Warming Climate. *Nat. Rev. Earth Environ.* 2, 628–644. doi:10.1038/s43017-021-00199-z

Ding, Q., Steig, E. J., Battisti, D. S., and Wallace, J. M. (2012). Influence of the Tropics on the Southern Annular Mode. *J. Clim.* 25, 6330–6348. doi:10.1175/Jcli-D-11-00523.1

Fogt, R. L., Bromwich, D. H., and Hines, K. M. (2011). Understanding the SAM Influence on the South Pacific ENSO Teleconnection. *Clim. Dyn.* 36, 1555–1576. doi:10.1007/s00382-010-0905-0

Held, I. M., and Soden, B. J. (2006). Robust Responses of the Hydrological Cycle to Global Warming. *J J. Clim.* 19, 5686–5699. doi:10.1175/jcli3990.1

Held, I. M., Ting, M., and Wang, H. (2002). Northern Winter Stationary Waves: Theory and Modeling. *J. Clim.* 15, 2125–2144. doi:10.1175/1520-0442(2002)015<2125:nwswta>2.0.co;2

Hitchman, M. H., and Rogal, M. J. (2010). ENSO Influences on Southern Hemisphere Column Ozone during the Winter to Spring Transition. *J. Geophys. Res.* 115, 12844. doi:10.1029/2009jd012844

Hoerling, M. P., Kumar, A., and Zhong, M. (1997). El Niño, La Niña, and the Nonlinearity of Their Teleconnections. *J. Clim.* 10, 1769–1786. doi:10.1175/1520-0442(1997)010<1769:enolna>2.0.co;2

Horel, J. D., and Wallace, J. M. (1981). Planetary-Scale Atmospheric Phenomena Associated with the Southern Oscillation. *Mon. Wea. Rev.* 109, 813–829. doi:10.1175/1520-0493(1981)109<0813:psapaw>2.0.co;2

Hu, K., Huang, G., Huang, P., Kosaka, Y., and Xie, S.-P. (2021). Intensification of El Niño-Induced Atmospheric Anomalies under Greenhouse Warming. *Nat. Geosci.* 14, 377–382. doi:10.1038/s41561-021-00730-3

Hu, K., Huang, G., Xie, S.-P., and Long, S.-M. (2019). Effect of the Mean Flow on the Anomalous Anticyclone over the Indo-Northwest Pacific in Post-el Niño Summers. *Clim. Dyn.* 53, 5725–5741. doi:10.1007/s00382-019-04893-z

Huang, P., and Xie, S.-P. (2015). Mechanisms of Change in ENSO-Induced Tropical Pacific Rainfall Variability in a Warming Climate. *Nat. Geosci.* 8, 922–926. doi:10.1038/ngeo2571

Jin, D., and Kirtman, B. P. (2009). Why the Southern Hemisphere ENSO Responses Lead ENSO. *J. Geophys. Research-Atmospheres* 114, D23101. doi:10.1029/2009jd012657

Karoly, D. J. (1989). Southern Hemisphere Circulation Features Associated with El Niño-Southern Oscillation Events. *J. Clim.* 2, 1239–1252. doi:10.1175/1520-0442(1989)002<1239:shcfaw>2.0.co;2

Kosaka, Y., and Nakamura, H. (2006). Structure and Dynamics of the Summertime Pacific-Japan Teleconnection Pattern. *Q.J.R. Meteorol. Soc.* 132, 2009–2030. doi:10.1256/qj.05.204

Kug, J.-S., An, S.-I., Ham, Y.-G., Kang, I.-S., and Climatology, A. (2010). Changes in El Niño and La Niña Teleconnections over North Pacific-America in the Global Warming Simulations. *Theor. Appl. Climatol.* 100, 275–282. doi:10.1007/s00704-009-0183-0

Lau, K.-H., and Lau, N.-C. (1992). The Energetics and Propagation Dynamics of Tropical Summertime Synoptic-Scale Disturbances. *Mon. Wea. Rev.* 120, 2523–2539. doi:10.1175/1520-0493(1992)120<2523:teapdo>2.0.co;2

Lau, N.-C., Leetmaa, A., Nath, M. J., and Wang, H.-L. (2005) Influences of ENSO-Induced Indo-Western Pacific SST Anomalies on Extratropical Atmospheric Variability during the Boreal Summer *J. Clim.* 18:2922–2942. doi:10.1175/Jcli3445.1

L'Heureux, M. L., and Thompson, D. W. J. (2006). Observed Relationships between the El Niño-Southern Oscillation and the Extratropical Zonal-Mean Circulation. *J. Clim.* 19, 276–287. doi:10.1175/jcli3617.1

Li, X., Holland, D. M., Gerber, E. P., and Yoo, C. (2015). Rossby Waves Mediate Impacts of Tropical Oceans on West Antarctic Atmospheric Circulation in Austral Winter. *J. Clim.* 28, 8151–8164. doi:10.1175/jcli-d-15-0113.1

Li, X., Cai, W., Meehl, G. A., Chen, D., Yuan, X., Raphael, M., et al. (2021). Tropical Teleconnection Impacts on Antarctic Climate Changes. *Nat. Rev. Earth Environ.* 2, 680–698. doi:10.1038/s43017-021-00204-5

Liu, Z., and Alexander, M. (2007). Atmospheric Bridge, Oceanic Tunnel, and Global Climatic Teleconnections. *Rev. Geophys.* 45. doi:10.1029/2005rg000172

Lu, J., Chen, G., and Frierson, D. M. W. (2008). Response of the Zonal Mean Atmospheric Circulation to El Niño versus Global Warming. *Glob. Warming J. Clim.* 21, 5835–5851. doi:10.1175/2008jcli2200.1

Meehl, G. A., Tebaldi, C., Teng, H., and Peterson, T. C. (2007). Current and Future U.S. Weather Extremes and El Niño. *Geophys. Res. Lett.* 34. doi:10.1029/2007gl031027

Mo, K. C., and Higgins, R. W. (1998). The Pacific-South American Modes and Tropical Convection during the Southern Hemisphere Winter. *Mon. Wea. Rev.* 126, 1581–1596. doi:10.1175/1520-0493(1998)126<1581:tpsama>2.0.co;2

Mo, K. C., and Paegle, J. N. (2001). The Pacific-South American Modes and Their Downstream Effects. *Int. J. Climatol.* 21, 1211–1229. doi:10.1002/joc.685

Müller, W. A., and Roeckner, E. (2008). ENSO Teleconnections in Projections of Future Climate in ECHAM5/MPI-OM. *Clim. Dyn.* 31, 533–549. doi:10.1007/s00382-007-0357-3

Power, S., Delage, F., Chung, C., Kociuba, G., and Keay, K. (2013). Robust Twenty-First-Century Projections of El Niño and Related Precipitation Variability. *Nature* 502, 541–545. doi:10.1038/nature12580

Rind, D., Chandler, M., Lerner, J., Martinson, D. G., and Yuan, X. (2001). Climate Response to Basin-specific Changes in Latitudinal Temperature Gradients and Implications for Sea Ice Variability. *J. Geophys. Res.* 106, 20161–20173. doi:10.1029/2000jd900643

Sardeshmukh, P. D., and Hoskins, B. J. (1988). The Generation of Global Rotational Flow by Steady Idealized Tropical Divergence. *J. Atmos. Sci.* 45, 1228–1251. doi:10.1175/1520-0469(1988)045<1228:tgogrf>2.0.co;2

Schneider, D. P., Okumura, Y., and Deser, C. (2012). Observed Antarctic Interannual Climate Variability and Tropical Linkages. *J. Clim.* 25, 4048–4066. doi:10.1175/Jcli-D-11-00273.1

Scott Yiu, Y. Y., and Maycock, A. C. (2019). On the Seasonality of the El Niño Teleconnection to the Amundsen Sea Region. *J. Clim.* 32, 4829–4845. doi:10.1175/Jcli-D-18-0813.1

Seager, R., Harnik, N., Kushnir, Y., Robinson, W., and Miller, J. (2003). Mechanisms of Hemispherically Symmetric Climate Variability*. *J. Clim.* 16, 2960–2978. doi:10.1175/1520-0442(2003)016<2960:mohscv>2.0.co;2

Simmons, A. J., Wallace, J. M., and Branstator, G. W. (1983). Barotropic Wave Propagation and Instability, and Atmospheric Teleconnection Patterns. *J. Atmos. Sci.* 40, 1363–1392. doi:10.1175/1520-0469(1983)040<1363:bwpaia>2.0.co;2

Straus, D. M., and Shukla, J. (2002). Does ENSO Force the PNA? *J. Clim.* 15, 2340–2358. doi:10.1175/1520-0442(2002)015<2340:deftp>2.0.co;2

Su, H., and Neelin, J. D. (2002). Teleconnection Mechanisms for Tropical Pacific Descent Anomalies during El Niño. *J J. Atmos. Sci.* 59, 2694–2712. doi:10.1175/1520-0469(2002)059<2694:Tmftpd>2.0.Co;2

Sun, B., Wang, H., and Zhou, B. (2019). Interdecadal Variation of the Relationship between East Asian Water Vapor Transport and Tropical Pacific Sea Surface Temperatures during January and Associated Mechanisms. *J. Clim.* 32 (21), 7575–7594. doi:10.1175/JCLI-D-19-0290.1

Sun, B., Wang, H., Li, H., Zhou, B., Duan, M., and Li, H. (2022). A Long-Lasting Precipitation Deficit in South China during Autumn-Winter 2020/2021: Combined Effect of ENSO and Arctic Sea Ice. *JGR Atmos.* 127, e2021JD035584. doi:10.1029/2021JD035584

Ting, M., and Yu, L. (1998). Steady Response to Tropical Heating in Wavy Linear and Nonlinear Baroclinic Models. *J. Atmos. Sci.* 55, 3565–3582. doi:10.1175/1520-0469(1998)055<3565:srtthi>2.0.co;2

Trenberth, K. E., Branstator, G. W., Karoly, D., Kumar, A., Lau, N.-C., and Ropelewski, C. (1998). Progress during TOGA in Understanding and Modeling Global Teleconnections Associated with Tropical Sea Surface Temperatures. *J. Geophys. Res.* 103, 14291–14324. doi:10.1029/97jc01444

Wang, Y., Huang, G., and Hu, K. (2020). Internal Variability in Multidecadal Trends of Surface Air Temperature over antarctica in Austral Winter in Model Simulations. *Clim. Dyn.* 55, 2835–2847. doi:10.1007/s00382-020-05412-1

Wang, Y., Hu, K., Huang, G., and Tao, W. (2021). Asymmetric Impacts of El Niño and La Niña on the Pacific-North American Teleconnection Pattern: the Role of Subtropical Jet Stream. *Environ. Res. Lett.* 16, 114040. doi:10.1088/1748-9326/ac31ed

Wang, Y., Huang, G., Hu, K., Tao, W., Li, X., Gong, H., et al. (2022). Asymmetric Impacts of El Niño and La Niña on the Pacific-South America Teleconnection Pattern. *Pattern J. Clim.* 35, 1825–1838. doi:10.1175/jcli-d-21-0285.1

Watanabe, M., and Kimoto, M. (2000). Atmosphere-ocean Thermal Coupling in the North Atlantic: A Positive Feedback. *Q.J R. Met. Soc.* 126, 3343–3369. doi:10.1002/qj.49712657017

Xie, S.-P., Hu, K., Hafner, J., Tokinaga, H., Du, Y., Huang, G., et al. (2009). Indian Ocean Capacitor Effect on Indo–Western Pacific Climate during the Summer Following El Niño. *J J. Clim.* 22, 730–747. doi:10.1175/2008jcli2544.1

Xie, S.-P., Kosaka, Y., Du, Y., Hu, K., Chowdary, J. S., and Huang, G. (2016). Indo-western Pacific Ocean Capacitor and Coherent Climate Anomalies in Post-ENSO Summer: A Review. *Adv. Atmos. Sci.* 33, 411–432. doi:10.1007/s00376-015-5192-6

Yang, S., Li, Z., Yu, J.-Y., Hu, X., Dong, W., and He, S. (2018). El Niño-Southern Oscillation and its Impact in the Changing Climate. *Natl. Sci. Rev.* 5, 840–857. doi:10.1093/nsr/nwy046

Yeh, S.-W., Cai, W., Min, S.-K., McPhaden, M. J., Dommenget, D., Dewitte, B., et al. (2018). ENSO Atmospheric Teleconnections and Their Response to Greenhouse Gas Forcing. *Rev. Geophys.* 56, 185–206. doi:10.1002/2017rg000568

Yuan, X. (2004). ENSO-related Impacts on Antarctic Sea Ice: a Synthesis of Phenomenon and Mechanisms. *Antartic Sci.* 16, 415–425. doi:10.1017/s0954102004002238

Yuan, X., and Martinson, D. G. (2000). Antarctic Sea Ice Extent Variability and its Global Connectivity*. *J. Clim.* 13, 1697–1717. doi:10.1175/1520-0442(2000)013<1697:asieva>2.0.co;2

Zhou, Z.-Q., Xie, S.-P., Zheng, X.-T., Liu, Q., and Wang, H. (2014). Global Warming-Induced Changes in El Niño Teleconnections over the North Pacific and North America. *J. Clim.* 27, 9050–9064. doi:10.1175/jcli-d-14-00254.1